SCIENCE AND TECHNOLOGY ORGANIZATION
CENTRE FOR MARITIME RESEARCH AND EXPERIMENTATION

Reprint Series **CMRE-PR-2019-031**

The ocean noise coherence matrix and its rank

Chris H. Harrison

May 2019

Originally published in:

The Journal of the Acoustical Society of America, volume 143, issue 3, March 2018, pp. 1689–1703 doi: https://doi.org/10.1121/1.5028360

About CMRE

The Centre for Maritime Research and Experimentation (CMRE) is a world-class NATO scientific research and experimentation facility located in La Spezia, Italy.

The CMRE was established by the North Atlantic Council on 1 July 2012 as part of the NATO Science & Technology Organization. The CMRE and its predecessors have served NATO for over 50 years as the SACLANT Anti-Submarine Warfare Centre, SACLANT Undersea Research Centre, NATO Undersea Research Centre (NURC) and now as part of the Science & Technology Organization.

CMRE conducts state-of-the-art scientific research and experimentation ranging from concept development to prototype demonstration in an operational environment and has produced leaders in ocean science, modelling and simulation, acoustics and other disciplines, as well as producing critical results and understanding that have been built into the operational concepts of NATO and the nations.

CMRE conducts hands-on scientific and engineering research for the direct benefit of its NATO Customers. It operates two research vessels that enable science and technology solutions to be explored and exploited at sea. The largest of these vessels, the NRV Alliance, is a global class vessel that is acoustically extremely quiet.

CMRE is a leading example of enabling nations to work more effectively and efficiently together by prioritizing national needs, focusing on research and technology challenges, both in and out of the maritime environment, through the collective Power of its world-class scientists, engineers, and specialized laboratories in collaboration with the many partners in and out of the scientific domain.

NOTE: The CMRE Reprint series reprints papers and articles published by CMRE authors in the open literature as an effort to widely disseminate CMRE products. Users are encouraged to cite the original article where possible.

The ocean noise coherence matrix and its rank

Chris H. Harrison[a)]
Emeritus Scientist, Centre for Maritime Research and Experimentation, Viale San Bartolomeo 400, 19126 La Spezia, Italy

(Received 9 December 2017; revised 6 March 2018; accepted 8 March 2018; published online 28 March 2018)

An expression for the cross-spectral density matrix of ocean noise naturally separates into a Toeplitz part and a Hankel part [Harrison (2017). J. Acoust. Soc. Am. **141**, 2812–2820]. The Toeplitz part is shown to be substantially rank-deficient for all practical acoustic cases, which has implications for adaptive beam forming. The influence of the Hankel part on passive fathometry is investigated, and its effect on adaptive beam forming is shown to be weak or negligible. Numerical demonstrations of these findings including beam patterns and eigenvalue spectra derived via circulant matrices are given based on a simple half-space with a Rayleigh reflection coefficient. Two sets of experimental data are revisited in this context, deriving eigenvalue spectra, beam patterns, and passive fathometry impulse responses with conventional and adaptive processing and differing amounts of averaging. The solution to a long-standing puzzle of processing inconsistency is suggested. © *2018 Acoustical Society of America*. https://doi.org/10.1121/1.5028360

[KTW] Pages: 1689–1703

I. INTRODUCTION

Ambient noise in acoustics is often regarded as a nuisance for sonar signal processing systems, and so its spectral and coherence properties have been studied in the context of separating it from a desired signal in order to reject it (Ainslie, 2010; Cron and Sherman, 1962; Buckingham, 1980; Kuperman and Ingenito, 1980; Harrison, 1996). In the last 15 years wind noise measured with a vertical array of hydrophones has been used in two ways as a tool to investigate the structure of the seabed. The first approach (Harrison and Simons, 2002) finds a reflection coefficient as a function of frequency and angle from the power ratio of an upward and downward steered beam, and thus depends on the noise's cross-spectral density matrix (CSDM) through the beam steering. The reflection properties can then be converted to layer properties by geoacoustic inversion (Quijano *et al.*, 2012; Yardim *et al.*, 2014) and in some cases can be converted to an impulse response by spectral factorization (Harrison, 2005). The second approach, known as "passive fathometry" (Siderius *et al.*, 2006; Harrison and Siderius, 2008), cross-correlates a vertical upward beam with a downward beam to find the local seabed's impulse response—a passive echo sounder. The entire operation can be done in the frequency domain and again relies on the noise's CSDM.

In a sense these two techniques both have the same aim, i.e., to deduce sound speed, density, absorption, and thickness for each of an arbitrary number of sub-bottom sediment layers, but their approaches are quite different. With a drifting vertical array they can also both produce a sub-bottom profile comparable with that of a boomer or echo sounder (see, e.g., Harrison, 2005; Siderius *et al.*, 2010). The aim of this paper is to investigate the mathematical properties of wind noise coherence and the CSDM that is used in these techniques.

It has already been pointed out (Harrison, 2017, 1996) that the theoretical shallow water noise CSDM with uniform hydrophone spacing, d, naturally separates into a Toeplitz part (a function of $n-m$) and a Hankel part (a function of $n+m$).

$$\begin{aligned} C_{n,m} = &\int_0^1 a(+s)a^*(+s)\exp(+ikd(n-m)s)ds \\ &+ \int_0^1 a(-s)a^*(-s)\exp(-ikd(n-m)s)ds \\ &+ \int_0^1 a(+s)a^*(-s)\exp(ikd(n+m)s)ds \\ &+ \int_0^1 a(-s)a^*(+s)\exp(-ikd(n+m)s)ds\,, \end{aligned} \tag{1}$$

where $s \equiv \sin\theta$ and the source amplitudes, a, are given by

$$\begin{aligned} &a(+s)a^*(+s) = 1, \\ &a(-s)a^*(-s) = VV^*, \\ &a(+s)a^*(-s) = V^*\exp(-i2kh), \\ &a(-s)a^*(+s) = V\exp(i2kh), \end{aligned} \tag{2}$$

with V being a (complex) seabed reflection coefficient, h being array height above the seabed, and having absorbed a factor of $\sin\theta/(1-VV^*)$ in each integral when compared with later equations.

Strangely the two methods depend on different aspects of the CSDM. The up-down power ratio approach is sensitive to the Toeplitz part rather than the Hankel part, whereas the passive fathometry approach is insensitive to the Toeplitz part and furthermore gives a null result without the Hankel part.

[a)]Visiting Professor at Institute of Sound and Vibration Research, University of Southampton, Highfield, Southampton SO17 1BJ, United Kingdom. Electronic mail: chris.harrison1946@gmail.com

In addition the beam forming in both cases can be performed using either conventional beam forming (CBF) or adaptive beam forming (ABF) methods. In the latter case one needs to invert the CSDM which means taking precautions against rank-deficiency. Thus one is driven to a set of interesting questions about the nature of ambient noise's CSDM, its symmetry, its invertibility, and how to optimise processing. Under what conditions is it rank-deficient and, in this case, how can ABF possibly work (for instance, reject shipping)? It was shown (Harrison, 2017) that it is possible to construct a separate Toeplitz and Hankel part from an experimental CSDM (although this is not equivalent to reducing an arbitrary Hermitian matrix to the sum of a Toeplitz and Hankel matrix).

In yet another application one might want to simulate a number of noise channels with a specified CSDM, and this can be done by applying Cholesky decomposition to the CSDM at each frequency and multiplying by random number sequences (Gentle, 1998), but this requires the CSDM to be strictly positive-definite, not just positive-semi-definite. Indeed, mathematically Cholesky decomposition is a standard test for positive-definiteness and so the positive-definite requirement would add another demand to the CSDM properties.

It is acknowledged that the answers to some of these questions may be known in other domains, for example, related fields of research include: reduced rank adaptive methods (Goldstein and Reed, 1997), ABF using multistage Wiener filters (Ricks *et al.*, 2001), and fast rank-reducing ABF (Fang *et al.*, 2014). Nevertheless, the objective of this paper is to collect related findings in the context of the two noise processing methods (i.e., up-down power ratio and passive fathometry), particularly in light of possible future developments to adapt them to function on moving platforms.

Section II investigates the behaviour of the Toeplitz part of the coherence matrix, arriving at a formula for its rank. Appendixes A and B spell out the relevant mathematics. Section III investigates the behaviour of the Hankel part of the matrix, distinguishing between the part that contains the seabed layering information and the part that may contribute to the calculation of minimum-variance-distortionless-response (MVDR) optimum hydrophone weights. Appendix C shows that, from an ABF point of view, the Hankel part usually has a negligible effect. Section IV contains some simulations of eigenvalues and beam patterns using fast Fourier transforms (ffts). Section V applies these findings to two sets of experimental data obtained with drifting vertical arrays.

II. THE RANK OF THE TOEPLITZ PART OF THE NOISE CSD MATRIX

CBF makes no demands on the rank of the CSDM, but ABF does since it has to invert the matrix, which means that it must either have full rank or precautions, or special techniques will be required to invert it. In practice the CSDM is often rank-deficient, and here the reasons for this are set out and a useful analytical expression for the rank derived. It will be shown that, on the contrary, for typical acoustic applications, where the array operates below its design frequency, the CSDM is *always* rank-deficient.

The summary below (with derivations in Appendixes A and B) assumes for the time being that the CSDM can be considered to be approximately Toeplitz, and that each element consists of an integral over all angles (potentially two angle dimensions) of the noise directionality (see Harrison, 1996, 2017).

To find the rank of a $N \times N$ Toeplitz matrix one has to calculate or at least estimate the behaviour of its eigenvalues, and this is quite straightforward numerically. However, to relate the rank to general features of ambient noise one needs an analytical approach which, despite the symmetry of the Toeplitz matrix, is not directly possible. There is an alternative using circulant matrices which have the convenient property that their eigenvalues are exactly their discrete Fourier transforms (DFTs), and the eigenfunctions for any circulant matrix are the columns of the matrix of Fourier exponential multipliers (the Vandermonde matrix, i.e., the complex Nth roots of unity).

A recipe for choosing an appropriate circulant matrix for the Toeplitz matrix in question and ensuring that it is indeed in some sense similar is given in a Tutorial by Gray (Gray, 2006), which summarizes earlier work (Gray, 1972). Gray's recipe offers two alternatives. The first is, using prior knowledge or a guess, to choose an appropriate circulant matrix (some suggestions are given in Appendix B), and to hope that under some conditions it will tend to the desired Toeplitz matrix. The second is to start with the function that was originally integrated to form the Toeplitz elements, namely, the noise directionality in this case. Gray shows that it is exactly this function that maps into the eigenfunction spectrum provided that the matrix is in some sense large as predicted by the Grenander-Szegö theorem (Grenander and Szegö, 1958). This latter approach for the ocean noise case is spelled out in Appendix A.

In summary, given a noise directionality $D(\sin\theta)$ and a uniformly spaced vertical array it is shown that the spectrum of the eigenvalues of the circulant matrix equivalent to $\mathbf{T}$ is exactly the N-point discretised noise directionality $D(\sin\theta) = D[(f_o/f)(\nu/N)]$, where ν is related to θ through $0 \le \nu \le N$ as $-1 \le \sin\theta \le +1$. This can be written as $D(\nu/\nu_o)$, where $\nu_o = Nf/f_o$. In other words, the distribution of eigenvalues mirrors the noise directionality function $D(\sin\theta)$ but scaled by $f_o/(Nf)$. The physical function $D(\sin\theta)$ (which is always positive since it is an acoustic power) has a beam width (to some defined lower limit), and, whether its discretised values are ordered or not, that width of significant values is unchanged and corresponds to ν_o. Note that in this context, since $\sin\theta$ can take values between -1 and $+1$, "beam width" means the fraction of the interval -1 to $+1$ occupied by noise of significant strength. Thus if D were to have the form of a positive angle boxcar of width w_p combined with a negative angle boxcar of width w_n this beam width would be $\sin\theta_b = (w_p + w_n)/2$.

The number of significant values in the eigenvalue spectrum is, by definition, the rank, so finally one arrives at

$$\text{rank}(\mathbf{T}) = 1 + \nu_o \sin\theta_b = 1 + N\frac{f}{f_o}\sin\theta_b, \tag{3}$$

where the additional one converts $\nu_o \sin\theta_b$ into an index.

The significance of Eq. (3) is that whenever the hydrophone array is practically usable acoustically, i.e., below the design frequency, $f \leq f_o$, there is little chance of the coherence matrix $\mathbf{T}$ achieving full rank even with a wide range of noise-source angles. Therefore palliatives such as "diagonal loading" are always necessary.

Some insight into the Grenander-Szegö theorem and Gray's recipe is given by the fact that multiplication of an arbitrary vector by a Toeplitz matrix can be interpreted as a filter or convolution operation. If the matrix is also circulant the result is a circulant convolution; there are also variants with a zero-padded vector and a "zero-padded" block matrix (meaning [**T 0**; **0 0**]). Clearly with any of these options the difference between a straight matrix multiplication and a circulant convolution becomes negligible as the end (or "edge") effects of the matrix disappear, as must happen when the matrix size tends to infinity.

III. THE INFLUENCE OF THE HANKEL PART ON THE CSDM

The third and fourth terms in Eq. (1) represent the coherently reflected paths whose interference behaves as normal modes. This is the region that Buckingham referred to as "inhomogeneous" (Buckingham, 1980). An important question is, does the addition of coherently related paths to the T-part (i.e., $\mathbf{R} = \mathbf{T} + \mathbf{H}$) have any influence on rank($\mathbf{R}$)? To answer this, first it is necessary to investigate $\mathbf{H}$ alone, although in the context of MVDR beamforming it is only the rank of $\mathbf{R}$ that matters in determining the optimum hydrophone weights. As far as passive fathometry is concerned, $\mathbf{H}$ has two important influences: one is the contribution to the MVDR weights, as just mentioned; the other is the part of $\mathbf{R}$ that is solely responsible for the impulse response of the sub-bottom layering (Harrison, 2017). A clear distinction and comparison of amplitudes can be made between these two contributions and the T-part by estimating the three integrals analytically with a crude half-space approximation for the reflection coefficient.

A. Relative amplitudes of matrix elements

The first two lines of Eq. (1) (i.e., the Toeplitz part, $T_{n,m}$) depend on the power reflection coefficient $|V|^2$ which is assumed to decay exponentially with $s\,(\equiv \sin\theta)$ from grazing up to the critical angle, and thereafter to take a fixed lower value, V_0. Writing the exponent in the integrals as

$$\phi_T = kd(n-m), \tag{4}$$

$T_{n,m}$ is

$$T_{n,m} = \int_0^1 \left\{\frac{s}{1-VV^*}\right\}[\exp(+i\phi_T s) + VV^*\exp(-i\phi_T s)]\,ds, \tag{5}$$

and if $|V|^2 = \exp(-\alpha\sin\theta)$ then $\sin\theta/(1-|V|^2) \approx 1/\alpha = 10\log_{10}(e)/\alpha_{\text{dB}}$ for angles less than critical but otherwise $\sin\theta/(1-|V|^2) \approx \sin\theta/(1-V_0{}^2)$, then

$$\begin{aligned} T_{n,m} \approx{}& \frac{1}{\alpha}\int_0^{s_c}[\exp(+i\phi_T s) + \exp(-(\alpha + i\phi_T)s)]\,ds \\ &+ \frac{1}{1-V_0{}^2}\int_{s_c}^1 [\exp(+i\phi_T s) \\ &+ V_0{}^2\exp(-i\phi_T s)]\,s\,ds. \end{aligned} \tag{6}$$

Although this can be evaluated exactly, all that is needed for comparison with the H-part is the value on the diagonal, i.e., $n = m$; $\phi_T = 0$,

$$T_{n,n} \approx \frac{2s_c}{\alpha} + \frac{(1+V_0{}^2)}{(1-V_0{}^2)}\frac{(1-s_c{}^2)}{2}. \tag{7}$$

Assuming that α is small (weak reflection decay with angle) the first term tends to dominate.

The Hankel part, $H_{n,m}$, [third and fourth lines of Eq. (1)] is

$$H_{n,m} = \int_0^1 \left\{\frac{s}{1-VV^*}\right\}[V\exp(+i\phi_H s) + V^*\exp(-i\phi_H s)]ds, \tag{8}$$

where the coefficients of s in the exponents are

$$\phi_H = k(2h - d(n+m)). \tag{9}$$

The complex reflection coefficient, up to the critical angle, can be represented by $V(s) = -\exp((i2kh_W - \alpha/2)s)$, where α is the angular decay constant, h_W is Weston's "effective depth," the displacement of an equivalent pressure release surface, $h_W = \rho/k\,s_c$ (see Harrison, 2010), where ρ is the relative density of the sediment. Since h_W is a small vertical displacement of the reflecting surface it can be added to the height of the array above the seabed to define

$$\phi_{HW} = k(2(h + h_W) - d(n+m)), \tag{10}$$

and so $H_{n,m}$ becomes

$$\begin{aligned} H_{n,m} \approx{}& \frac{-2}{\alpha}\int_0^{s_c}\exp(-\alpha s/2)\cos(\phi_{HW}\,s)\,ds \\ &+ \frac{2V_0}{1-V_0{}^2}\int_{s_c}^1 \cos(\phi_H\,s)\,s\,ds \\ \approx{}& \frac{-2\exp(-\alpha s_c/2)}{\alpha\,(\phi_{HW}{}^2 + \alpha^2/4)}(\phi_{HW}\sin(\phi_{HW}s_c) \\ &- (\alpha/2)\cos(\phi_{HW}s_c)) \\ &+ \frac{2V_0}{1-V_0{}^2}\left\{\frac{(\sin(\phi_H) - s_c\,\sin(\phi_H\,s_c))}{\phi_H}\right. \\ &\left.+ \frac{(\cos(\phi_H) - \cos(\phi_H\,s_c))}{\phi_H{}^2}\right\}, \end{aligned} \tag{11}$$

or rearranging in terms of sinc functions $H_{n,m}$ is

$$H_{n,m} \approx \frac{-2\,s_c \exp(-\alpha s_c/2)}{\alpha} \frac{{\phi_{HW}}^2}{({\phi_{HW}}^2 + \alpha^2/4)} \times \left(\mathrm{sinc}(\phi_{HW} s_c) - \left(\frac{\alpha s_c}{\phi_{HW}}\right) \cos(\phi_{HW} s_c) \right) + \frac{V_0\,(1-{s_c}^2)}{1-{V_0}^2} \left\{ \mathrm{sinc}\left(\frac{(1+s_c)\phi_H}{2}\right) \times \cos\left(\frac{(1-s_c)\phi_H}{2}\right) + \mathrm{sinc}\left(\frac{(1-s_c)\phi_H}{2}\right) \cos\left(\frac{(1+s_c)\phi_H}{2}\right) + \mathrm{sinc}\left(\frac{(1+s_c)\phi_H}{2}\right) \mathrm{sinc}\left(\frac{(1-s_c)\phi_H}{2}\right) \right\}. \quad (12)$$

This shows that each term contains at least one factor proportional to $1/\phi_H$ which is of order $1/(2kh)$. Thus the ratio of $T_{n,n}$ to $H_{n,n}$ has modulus

$$\left| \frac{H_{n,n}}{T_{n,n}} \right| \approx \frac{1}{2kh}, \quad (13)$$

but $H_{n,n}$ oscillates about zero along the diagonal with zero separations given by $\Delta n = dn/d\phi_H = 1/(2k\,d\,s_c)$, and from frequency to frequency with zero separations at $\Delta f = df/d\phi_H = 1/(2k\,h\,s_c)$. There is also the possibility of slow beating caused by the small difference between ϕ_H and ϕ_{HW}. At the design frequency (e.g., 4.167 kHz in the experiments described later) the ratio in Eq. (13) reduces to $d/(2\pi h)$ which for $d = 0.18$ m and $h = 50$ m is 5.7×10^{-4}; however, for lower frequencies or closer to the seabed it will be larger and not necessarily negligible. Note that all oscillations in the tails of the sinc functions are caused by the assumption of a sharp edge at the critical angle. A more realistic reflection model would have a more gradual transition which tends to reduce the oscillation dramatically.

In contrast, the vertical component of **H** that contains all the seabed information is from between $\theta = \pi/2$ and $\theta = \pi/2 - \Delta$, i.e., s between 1 and $\cos\Delta$,

$$H^{CC}_{n,m} = \int_{\cos\Delta}^{1} \left\{ \frac{s}{1 - VV^*} \right\} [V^* \exp(+i\phi_H\, s) + V \exp(-i\phi_H\, s)]\, ds \approx \frac{2V_0}{1-{V_0}^2} \int_{\cos\Delta}^{1} \cos(\phi_H\, s)\, s\, ds \approx \frac{2V_0\ \cos(\phi_H)}{1-{V_0}^2} (1-\cos\Delta) \approx \frac{V_0\ \cos(\phi_H)\,\Delta^2}{1-{V_0}^2}. \quad (14)$$

The width of the effective area after cross-correlation depends on the time resolution which, in turn, depends on the bandwidth (i.e., the design frequency). This width is the Fresnel zone size [Harrison and Siderius, 2008, Eq. (A8)] so that the effective angle is $\Delta = \sqrt{\lambda/r}$, where λ is the design wavelength ($\lambda = 2d$) and r is the depth of the receiver.

Although Δ is much smaller than the angle spread in Eq. (12), that same spread is the cause of the $1/2hk$ factor in H that is absent in H^{CC}. Surprisingly the resulting ratio [excluding the first term of Eq. (12)] is not necessarily big or small

$$\frac{H^{CC}_{n,n}}{H_{n,n}} \approx \frac{1}{2}\frac{h}{r}\, kd. \quad (15)$$

The $\cos(\phi_H)$ term, if Fourier transformed, is the impulse response of the seabed which in this case, having assumed a half-space, is a delta function at two-way path length $2h$. Excluding this term the ratio of $H^{CC}_{n,n}$ to $T_{n,n}$ is

$$\frac{H^{CC}_{n,n}}{T_{n,n}} \approx \frac{V_0\alpha}{(1-{V_0}^2)s_c}\frac{d}{r}. \quad (16)$$

For example, with $\alpha = 0.2303$, i.e., $\alpha_{\mathrm{dB}} = 1$ dB/rad; $V_0 = 0.1$; $s_c = 0.2$; $d = 0.18$ m; $r = 50$ m, the ratio is 4.2×10^{-4}.

B. Matrix rank

1. The rank of H

The oscillatory behaviour of Eq. (12) shows that trace(**H**) (i.e., $\sum \lambda^H_n$) passes through zero at regular frequency intervals, and so there must be some positive and negative eigenvalues for their sum to equate to zero; in fact, typically the eigenvalues of a periodic Hankel matrix are positive and negative pairs. Furthermore a truly periodic real Hankel matrix can be shown to have rank two. Equation (12) shows that even in the simple case of a half-space there are several clustered frequency components but with one dominating, so rank(**H**) is expected to be small.

2. The rank of (T + H) for ABF purposes

Since trace(**T** + **H**) = trace(**T**) + trace(**H**), the fact that trace(**H**) oscillates about zero means that there are some acoustic frequencies where the sum of the eigenvalues of **T** + **H** is equal to the sum of the eigenvalues of **T**,

$$\sum_{i=1}^{N} \lambda_i^{T+H} = \sum_{i=1}^{N} \lambda_i^{T} + \sum_{i=1}^{N} \lambda_i^{H} \Rightarrow \sum_{i=1}^{N} \lambda_i^{T}, \quad (17)$$

and since at all frequencies the matrices **T** + **H** and **T** are both positive-semi-definite their eigenvalues are never negative,

$$\lambda_i^{T+H} \geq 0; \quad 1 \leq i \leq N,$$
$$\lambda_i^{T} \geq 0; \quad 1 \leq i \leq N,$$

meaning that there is little leeway for differences, i.e., the influence of **H** on the rank of (**T** + **H**) is small. Some useful inequality relations are collected in Appendix C with a demonstration that the standard deviation of the differences is small compared with the mean eigenvalue, and the individual differences are much smaller than the largest eigenvalue.

3. The distinction between natural T and H parts and artificially separated T and H parts

Section I referred to the Toeplitz and Hankel parts that appear naturally in the usual formulation of noise coherence as in Eqs. (1), (5), and (8). Harrison (2017) showed that, starting from an experimental CSDM, one could extract matrices that were, by definition, Toeplitz (by summing elements along the diagonals) or Hankel (by summing along the anti-diagonals). It is important to note that the latter type of matrices do not have the same rank properties as the "natural" ones, as is easily demonstrated.

A Toeplitz matrix can be constructed by matrix-multiplying the column vector, $x_n = \exp(iAn)$ by its conjugate transpose. This automatically has rank one because each row is a multiple of the first row. However, if the elements are summed along each diagonal the number of elements in the jth diagonal is $N - |j|$ and consequently the (constant) values down each diagonal are multiplied by $N - |j|$. Therefore each row is no longer a multiple of the other rows, and the matrix is potentially full rank. In contrast, taking the mean, as opposed to the sum, down each diagonal has no such effect since, with a Toeplitz matrix there is no change to its elements.

Similarly a Hankel matrix with rank one can be formed by multiplying the same vector by its unconjugated transpose. In the same way, summing down the anti-diagonals potentially increases the rank to full.

In summary, summing down the diagonals or anti-diagonals will always alter the rank whereas averaging has no effect for pure Toeplitz or pure Hankel matrices. However, such averaging of an experimental CSDM (i.e., not exactly Toeplitz or Hankel) may still alter its rank.

IV. SIMULATIONS

Equations (1), (5), and (8) form a convenient basis for simulation and numerical demonstration of the analytical findings of Secs. II and III. Excluding the exponential terms the integrand of Eq. (5) constitutes the noise directionality [as a function of $\sin(\theta)$] corresponding to the Toeplitz part. The solid line in Fig. 1 shows this directionality assuming the Rayleigh reflection coefficient for V with the following seabed parameters, none of which is particularly critical: sound speed 1600 m/s (critical angle $\theta_c = 20.36°$); specific gravity 1.5; volume absorption 0.1 dB/λ. Mathematically there can be no equivalent beam pattern for H [Eq. (8)] since the matrix is not positive-semi-definite [i.e., $\mathbf{v}^\dagger\mathbf{H}\mathbf{v}$ may be positive or negative, as we will see in Fig. 2(b)]. Physically, in the construction of the noise coherence formula [Eqs. (1), (5), and (8)] the two H terms each come from an up-going and a down-going pair of angles. In other words neither term corresponds to a single direction. In contrast the matrix $(\mathbf{T} + \mathbf{H})$ is always positive semi-definite since $\mathbf{v}^\dagger(\mathbf{T} + \mathbf{H})\mathbf{v}$ corresponds physically to a power.

Solving the integrals numerically, assuming the Rayleigh reflection formula, the complete Toeplitz and Hankel matrices can be formed, and then the eigenvalues and singular values of each matrix and their sum can be found using proprietary algorithms. Geometric and processing parameters are assumed

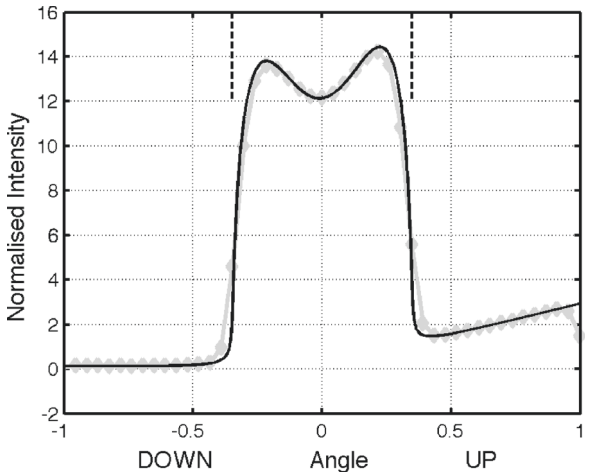

FIG. 1. Directionality from the envelope of Eq. (5) (solid line), and from the Fourier transform of a conjugate-symmetric version of the first row of $\mathbf{T}$ (gray connected dots). The two vertical bars indicate the sine of the critical angle, s_c.

to be height above seabed $h = 20$ m; hydrophone separation $d = 0.18$ m (i.e., design frequency = 4167 Hz; number of hydrophones $N = 32$; acoustic frequency $f = 3000$ Hz). Figure 2(a) shows a linear plot of the eigenvalue spectrum for T, with that of (T + H) superimposed. Figure 2(b) shows the spectrum for H—note the large difference in scale and the fact that eigenvalues come approximately in positive/negative pairs. The three vertical bars in Fig. 2(a) indicate the expected eigenvalue indices that tally with the significant beam widths according to Eq. (3). The left-most corresponds to the more or less rectangular beam out to the critical angle, $1 + Nf/f_o \sin(\theta_c)$; the middle one corresponds to the non-critical remainder of the beam, $1 + Nf/f_o\ (1 - \sin(\theta_c))$; and the right-most one is the ultimate limit of 90°, $1 + Nf/f_o$, seen more clearly in the log plot of Fig. 2(c). Figure 3 shows that the eigenvalue spectrum changes with acoustic frequency according to Eq. (3).

In addition one can form a circulant matrix $\mathbf{C}$ from a conjugate symmetric version of the first row of $\mathbf{T}$ (i.e., $T_{CS} = [T_{1,1}\ T_{1,2}\ T_{1,3}...\ T_{1,N}\ 0\ T_{1,N}^*.\ T_{1,2}^*]$) which has the property that the elements of its Fourier transform are the same as the eigenvalues of $\mathbf{C}$ (see Appendixes A and B). Figure 4(a) shows that this relation is numerically true by comparing the (64-point) Fourier transform of T_{CS} with the eigenvalues of $\mathbf{C}$, with both quantities being ordered according to their magnitude. Figure 4(b) shows that, as one might suspect, the same Fourier transform (having extracted 32 alternate points, see Appendix B) is quite close to the eigenvalues of $\mathbf{T}$, but agreement is not exact.

Last, performing an inverse Fourier transform of the same first row T_{CS} naturally leads back to the original directionality. This is shown as the connected-dots-line superimposed on the original beam pattern in Fig. 1. Furthermore performing the same operation on (T + H) for values of h greater than about 10 m, so that the influence of H is sufficiently small, leads to a beam pattern that is within a line width in Fig. 1, and for that reason, not shown.

This latter operation with simulated data is trivial, but with the experimental data in Sec. V it is not trivial, because

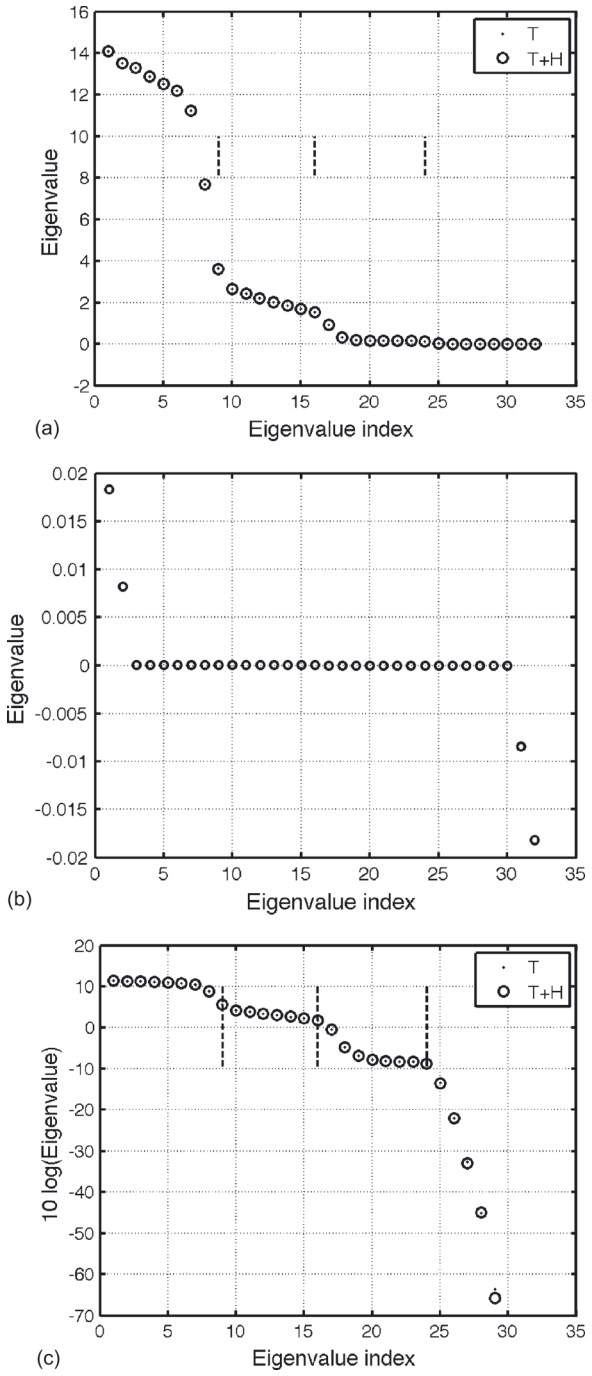

FIG. 2. (a) Linear scale eigenvalue spectrum of **T** (dots) and (**T** + **H**) (circles) showing that they are both positive semi-definite, and that they agree closely. The vertical bars indicate the indices corresponding to $N \times fl/f_o$ times, respectively, s_c, $(1 - s_c)$, and 1. (b) Linear scale eigenvalue spectrum for **H** alone showing positive and negative pairs of eigenvalues. (c) Eigenvalues identical to (a) except for the logarithmic scale which emphasises the minor differences between the spectra of **T** (dots) and (**T** + **H**) (circles). The vertical bars indicate the indices corresponding to $N \times fl/f_o$ times, respectively, s_c, $(1 - s_c)$, and 1.

the experimental noise directionality is unknown. In fact this way of obtaining the noise directionality is a practical and computationally efficient alternative to the usual one of beam forming via CSDM since it only requires a single Fourier transform of the first row of the CSDM [as opposed to the N $(N + 1)$ multiplications for *each beam* required for $\mathbf{v}^\dagger\mathbf{C}\mathbf{v}$].

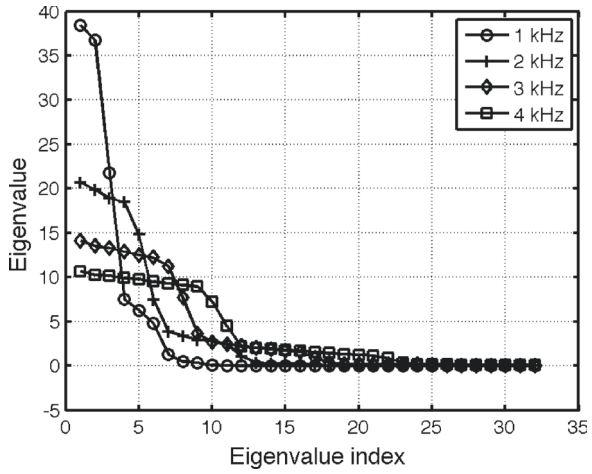

FIG. 3. Linear eigenvalue spectra at four frequencies showing the behaviour predicted by Eq. (3).

V. DEMONSTRATIONS WITH EXPERIMENTAL DATA

A. Experimental data from 2003 and 2004

Two experiments were carried out with the same 32-element drifting vertical array in the Mediterranean near the

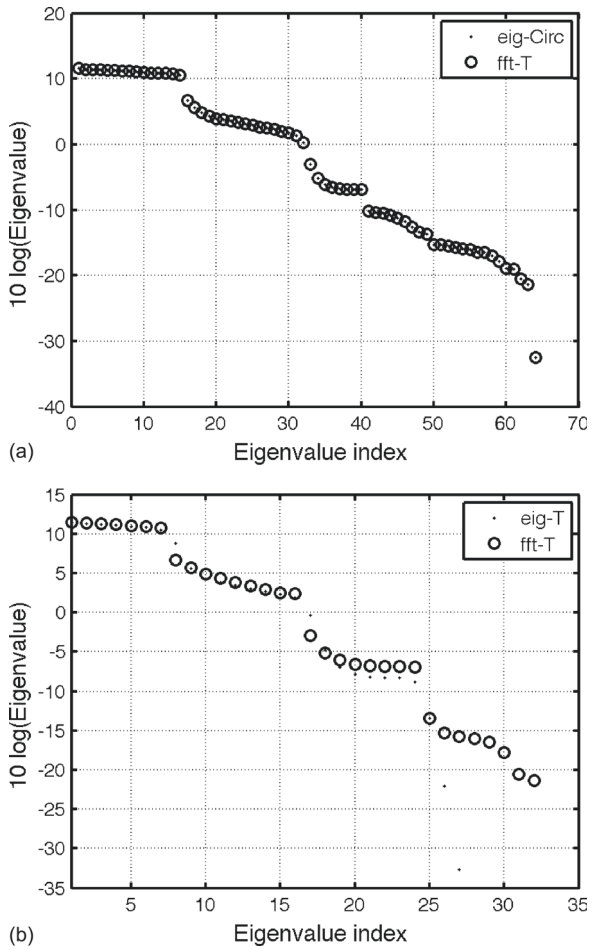

FIG. 4. (a) Exact agreement between the eigenvalues of the circulant matrix constructed from **T** evaluated with proprietary software (dots), and the Fourier transform of its first row, i.e., a conjugate symmetric version of the first row of **T** (circles). (b) Slight disagreement between the eigenvalues of **T** evaluated with proprietary software (dots), and alternate points from the Fourier transform of a conjugate symmetric version of the first row of **T** (circles).

Ragusa Ridge, already described in detail (Harrison and Siderius, 2008; Harrison, 2005). The 2003 experiment was over a relatively smooth layered seabed and the sea surface had "white horses" providing wind and wave noise but no swell. In contrast the 2004 data had a strong swell causing the array to bob up and down with an amplitude of about 1 m and a period of 7 s (Harrison, 2017; Traer and Gerstoft, 2011) and the seabed consisted of shallow pools of sediment over the rock of the Ragusa Ridge. The array had a hydrophone separation of 0.18 m giving a design frequency of 4167 Hz, and noise was sampled at 12 kHz.

A long-standing puzzle (for this author) has been why the two drifting 32-element-array data sets obtained in 2003 and 2004 in similar areas but very different weather conditions (Harrison and Siderius, 2008) respond so inconsistently to processing. This puzzle has largely been the inspiration for this paper and Harrison (2017), and a possible explanation is offered in Sec. V B below. The puzzle is that the 2003 data (white horses but not particularly rough sea) requires long averaging time and ABF to produce a clear bottom return and sub-bottom two-way penetration of 50 m (Harrison, 2008; Siderius *et al.*, 2010), whereas the 2004 data (very rough sea; seabed of sand pools over rock) required only 4 overlapping 4096 length ffts to produce a clear bottom return and sub-bottom two-way penetration of 4 m to rock using only conventional beamforming (Harrison, 2017; Traer and Gerstoft, 2011). In the latter case motion of the array precluded the necessary integration time of ABF processing.

B. Experimental directionality

The noise directionality depends dramatically on the sound speed profile and the depth of the array as well as the reflection losses of the seabed and the sea surface. In particular this affects the balance between the residual of the wave source dipole [s in the numerator of Eq. (5)] and the cumulative multipath effect $(1-|V|^2)$ in the denominator of Eq. (5), see examples in Harrison (1996, 2004). With large bottom losses (i.e., $V=0$) or absence of ducted propagation Eqs. (1) and (5) revert to those of Cron and Sherman (1962), and the noise is proportional to $\sin(\theta)$ in the upward direction but zero downwards.

Figure 5(a) is a plot of noise intensity vs frequency and angle for 2003, derived in the same way as Fig. 1 by taking the Fourier transform of the conjugate symmetric first row of the Toeplitz-separated part of the CSDM. At the design frequency (where $kd=\pi$) the transform pair is hydrophone number, n, and $s=\sin\theta$. At lower frequencies the transform needs to be interpolated from s to sf/f_o to account for the factor kd in the exponent [see, e.g., Eqs. (4) and (5)]. There is a clear "noise notch," a simple frequency-independent downward-refraction effect resulting in an absence of noise within about 12° of horizontal, but for upward angles an apparently uniform spread, and for downward angles a weaker spread.

In contrast, Fig. 5(b) for the 2004 data has a general decay from vertically upward to vertically downward with a pronounced superimposed horizontal peak. The angular

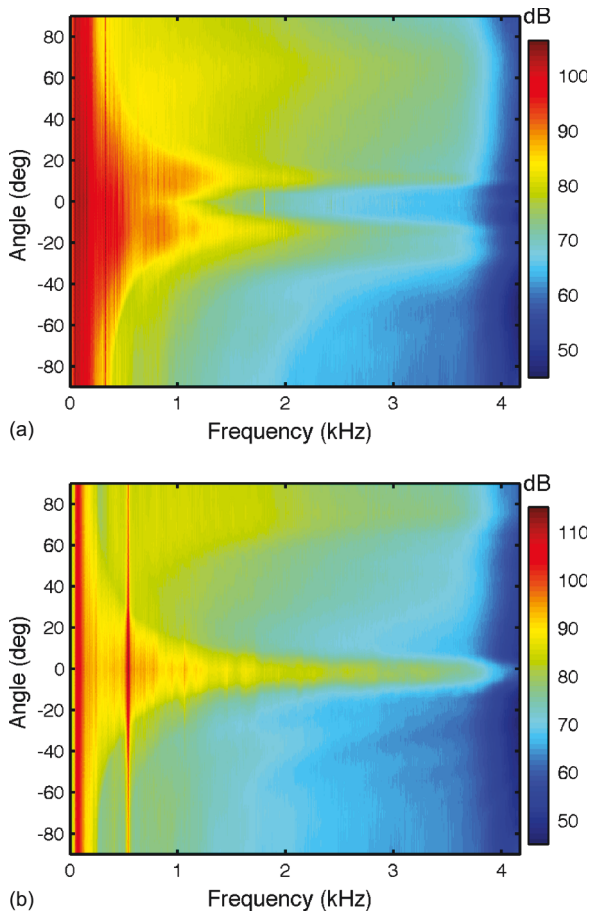

FIG. 5. (Color online) (a) Intensity vs angle and frequency for 2003 data. (b) Intensity vs angle and frequency for 2004 data.

variation for both data sets can be compared more clearly at spot frequencies in Fig. 6 (solid line for 2004; dashed line for 2003). In Figs. 5 and 6 the intensity scale is arbitrary, but identical equipment and processing was used in the two experiments. In Fig. 6 it can be seen that the variation above horizontal in both cases is more or less linear, i.e., proportional to $\sin\theta$. There is a noticeable spike at the upward vertical for 2004, and this is thought to be the sound of waves hitting the surface buoy, to which the array was loosely attached (see Harrison, 2008). In fact, by listening and comparing time domain beamformed endfire and broadside beams, one can hear this distinctly. One can also hear that the central peak is a single nearby ship which is responsible for the strong spectral line at about 500 Hz in Fig. 5(b). The residual noise in 2004 resembles the high bottom (and surface) loss case probably caused by rocky seabed and strong surface swell.

Figure 6, for 2004, shows that it is certainly true that there is a strong source vertically above the array, regardless of its nature. In that case, notwithstanding the detection and proof of 7-s-period vertical motion of the array (Traer and Gerstoft, 2011; Harrison, 2017), the "good" results of the cross-correlation technique (i.e., producing a clear impulse response) could possibly be deemed fortuitous in that example on the grounds that not much integration time would have been required with the sound source so favourably placed. Nevertheless this would explain the aforementioned

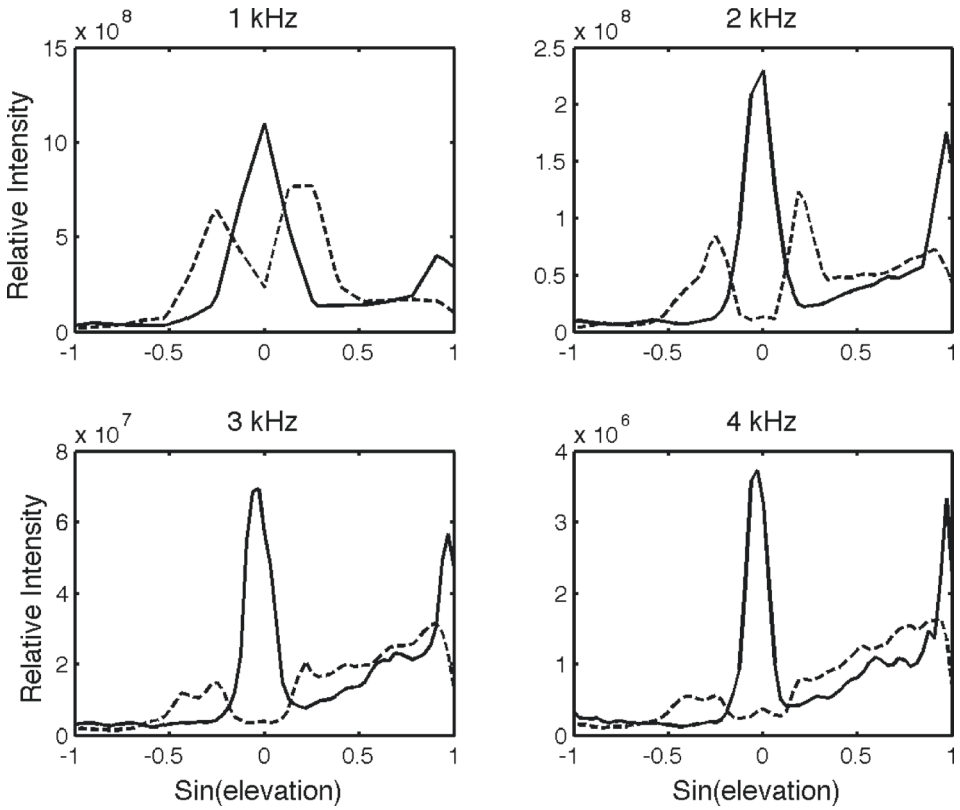

FIG. 6. Superimposed intensity vs angle for the 2003 (dashed line) and 2004 (solid line) data at four frequencies as indicated: 1, 2, 3, and 4 kHz.

puzzle, that a short integration time was sufficient in bad weather with a rocky seabed, but a long integration time was required in good weather over deep-layered sediments.

C. Experimental eigenvalues

To investigate the experimental eigenvalue behaviour three matrices are estimated by averaging the outer product of the Fourier transforms of the hydrophone channels: the standard coherence matrix, **R**; the separated Toeplitz part, **T**; the separated Hankel part, **H** ("separated" as defined in Harrison, 2017). Each of these quantities is averaged over 500 overlapping 4096-blocks (85 s at 12 kHz sampling), and each is a 32-by-32 matrix and a function of 2048 frequencies (up to Nyquist at 6 kHz).

A composite plot of eigenvalue spectra for 2003 is shown in Fig. 7(a) for six frequencies. The equivalent for 2004 is shown in Fig. 7(b). In all cases the actual step (expected location marked by the vertical line), though in the correct place at all frequencies, is less dramatic than implied by the theory of Sec. II and Appendix A or Figs. 2(a) and 2(c). However, as already pointed out in Harrison (2017), this is likely to be because even after extensive averaging the true coherence is contaminated by unwanted angular cross-terms which result effectively in addition of some randomness to the matrices.

As a palliative it might be thought to be possible to truncate the eigenvalue spectrum at a point defined by a factor times the limit given in Eq. (3), as indicated in the figures. However, in practice, even allowing an "engineering percentage correction" to this factor there appears to be no obvious benefit.

D. Impulse response plots

Figures 8(a) and 8(b) show impulse responses for all permutations of experiment year (2003 or 2004), and processing (CBF or ABF using MVDR with optimum weights based on the separated Toeplitz part). Figure 8(a) is the result of 40 averaged blocks whereas Fig. 8(b) is for 500 blocks. In both experiments a two-way path of about 110 m was expected.

It is striking that, in the upper panels of Fig. 8(a) with CBF and only 40 blocks the 2004 data have an extremely clear peak while the 2003 data have no visible bottom arrival at all. Note that there are various irrelevant artefacts at about 5 and 20 m (see Harrison and Siderius, 2008 for details). In contrast, in the lower panels of Fig. 8(a), using ABF, the 2004 data are hardly altered but the 2003 data begins to respond weakly.

Increasing the number of blocks to 500 with CBF processing, the upper panels of Fig. 8(b) shows that there is limited improvement in 2003, and the amplitude of the 2004 peak has just about halved. But the latter point is because the periodic motion of the array has distributed the arrivals into two separate peaks which are easily seen when enlarged. In the lower two panels the 2004 peak is largely unchanged by ABF processing, but on the other hand, the 2003 data are very much improved by ABF processing.

VI. CONCLUSIONS

Surprisingly, ocean ambient noise contains a lot of useful information, not least about the ocean upper and lower boundaries, but in particular about sub-bottom layering. Several methods are available for extraction and processing of this information, but they all rely on the noise coherence,

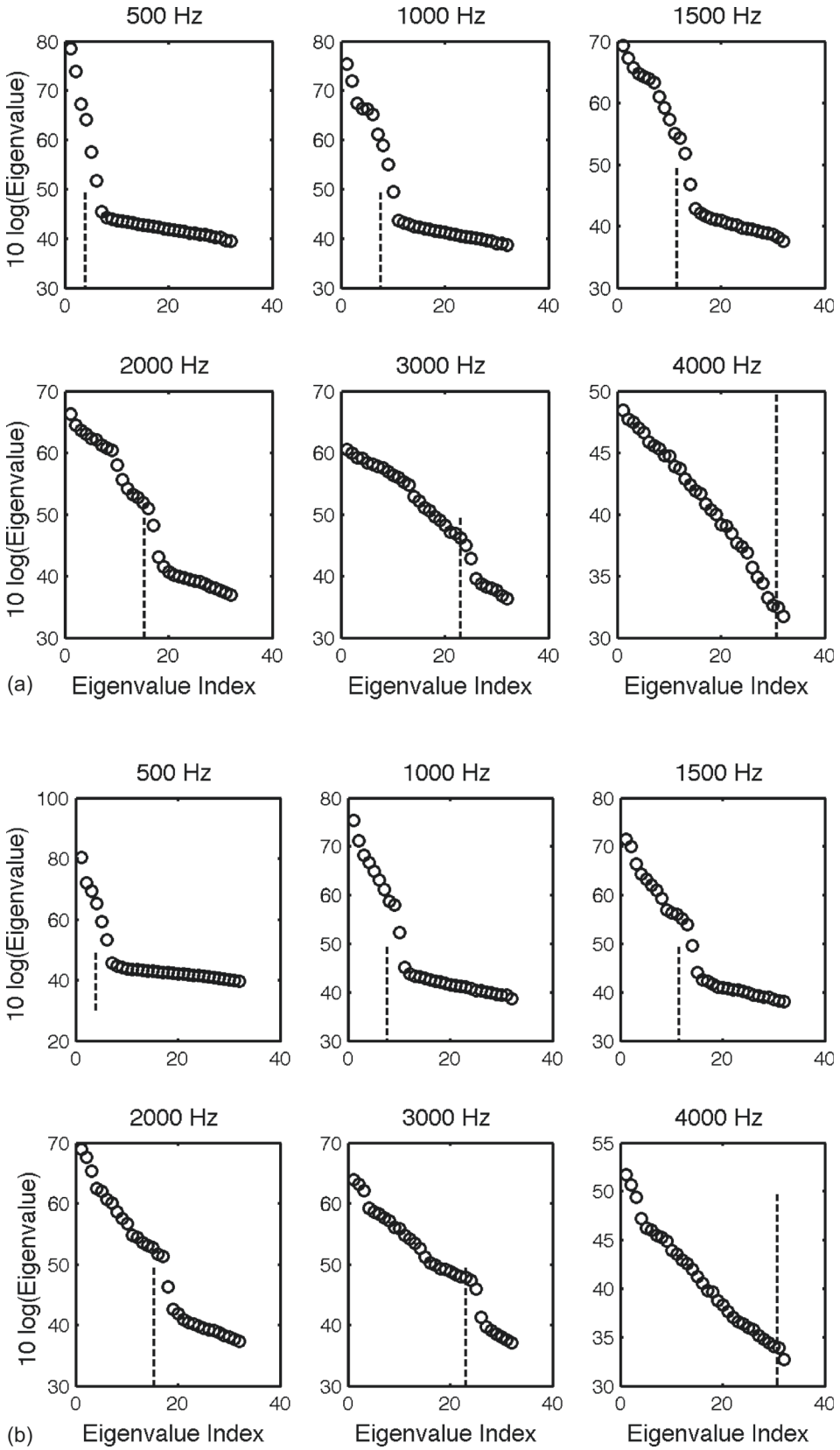

FIG. 7. (a) Eigenvalue spectra for 2003 data with a 500 block average at six indicated frequencies. The locations of the expected step [limit set by Eq. (3)] are shown by the vertical dashed lines. (b) Eigenvalue spectrum for 2004 data with a 500 block average at six indicated frequencies. The locations of the expected step [limit set by Eq. (3)] are shown by the vertical dashed lines.

i.e., the frequency-dependent CSDM for a hydrophone array. Because there is always conflict between the necessity for some kind of time-averaging and temporal changes in the environment or hydrophone locations, an understanding of this quantity is paramount. This paper has addressed the questions of its separation into a Toeplitz and a Hankel part, the eigenvalue behaviour of both parts, their rank, and associated beam patterns.

An analytical treatment of the Toeplitz part in Sec. II showed that whenever the hydrophone array is practically usable acoustically, i.e., below the design frequency, the coherence matrix is necessarily rank-deficient [Eq. (3)], and

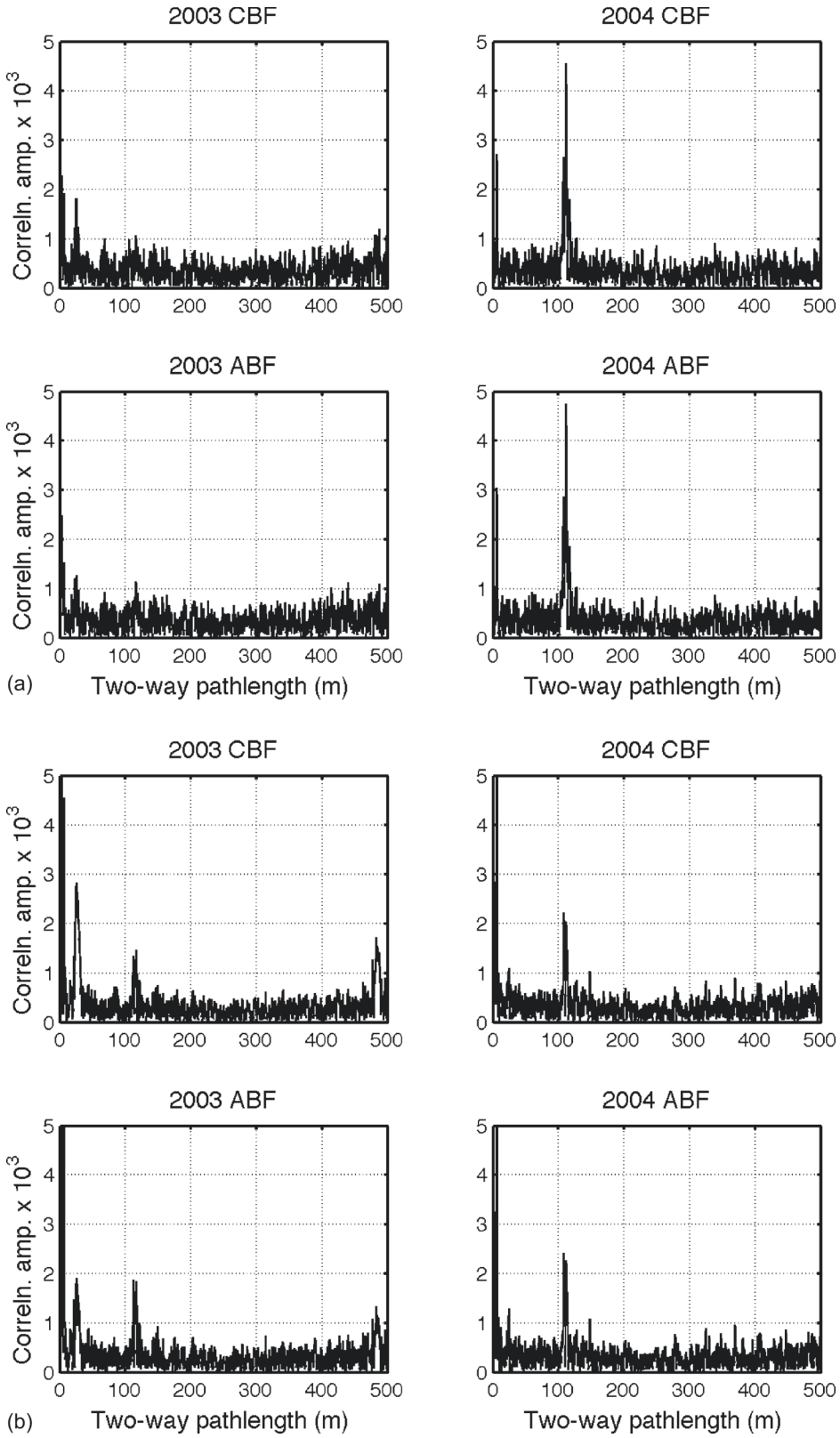

FIG. 8. (a) Impulse responses for the 2003 and 2004 data each using CBF and ABF processing, as indicated, with a 40 block average. (b) Impulse responses for the 2003 and 2004 data each using CBF and ABF processing, as indicated, with a 500 block average.

so adaptive methods that rely on matrix inversion require palliatives such as diagonal loading. Even if averaging raises the rank to a point sufficient for matrix inversion, still the true coherence matrix will be contaminated by angular cross-terms. These findings were based on setting up a circulant matrix, which is in some sense similar to the given Toeplitz matrix and then using the property that the fft of its first row is identical to its eigenvalues. A derivation was given in Appendix A, and some candidate circulant matrices given in Appendix B. This eigenvalue spectrum without any rearrangement is the same shape as the originally assumed noise directionality, and when sorted in descending order it is the same as the eigenvalue or singular value spectrum calculated with proprietary software.

To investigate behaviour of the Hankel part the specific case of a half-space bounded by a seabed with Rayleigh reflection coefficient was taken in Sec. III. Analytical solutions for the Hankel [Eqs. (8), (12), and (14)] and Toeplitz terms [Eqs. (5) and (7)] were given. It was shown that the Hankel part, paradoxically, contains *all* the sub-bottom layering information that is used by passive fathometry, but still it is usually weak enough that adding it to the Toeplitz part does not significantly alter the eigenvalues or rank. In other words the eigenvalue spectrum of $(\mathbf{T}+\mathbf{H})$ is more or less the same as that of $\mathbf{T}$ alone. Appendix C used the Weyl inequalities and some other relations to demonstrate this. Limits on the rough ratio of Hankel to Toeplitz terms were given for the passive fathometry case [Eq. (16)] and for ensuring minimal influence on the eigenvalue spectrum [Eq. (13)].

Section IV took the Rayleigh reflection case as the basis for some numerical simulations and demonstrations of the analytical findings. Figures 1–4 collected various properties including beam pattern and eigenvalue spectra as a function of frequency. Good agreement was found with the formula for rank [Eq. (3)] by marking the expected stepping points in the spectra [Figs. 2(a) and 2(c)].

Section V revisited two sets of drifting array experimental data (Fig. 5) in light of these predictions and in light of a long-standing "puzzle." The puzzle was that in unfavourable weather and environmental conditions CBF processing worked well with minimal averaging and indeed revealed array periodic vertical motion, whereas with favourable environment and weather conditions CBF did not work and ABF was required to get any impulse response at all. It is thought that the reason for the processing performing well in the poor conditions is that, for whatever reason, but probably waves splashing on the buoy in a heavy sea, the noise contained a strong sound source overhead (Fig. 6). This angular concentration of sound, particularly in that direction, strongly reduces the integration time required for the impulse response to emerge.

Figure 7 shows that there is indeed a step in the eigenvalue spectrum as predicted by Eq. (3), but in practice it takes a lot of averaging to see it. This is because angular cross-terms contaminate the true coherence matrix. The end-product impulse responses (Fig. 8) demonstrates the "puzzling" behaviour explicitly.

ACKNOWLEDGMENTS

In his Emeritus capacity the author thanks CMRE for continuing to provide work facilities. He also thanks the Chief Scientist during the experiments, Peter Nielsen, and the Captain and crew of the NRV Alliance.

APPENDIX A: THE EIGENVALUE SPECTRUM OF A TOEPLITZ MATRIX

Appendix B suggests some appropriate circulant matrices without considering the similarity of their eigenvalue spectra to that of the given Toeplitz matrix $\mathbf{T}$. According to the Grenander-Szegö theorem (Grenander and Szegö, 1958) similarity is assured when the matrix (i.e., N) is large in some sense. This theorem is embedded in a recipe due to Gray (2006, Sec. 4.4) where, rather than guessing candidate circulant matrices, one starts with the continuous function that, when integrated produces the Toeplitz elements T_{nm}—in the noise coherence case this function is none other than the noise directionality. Then the recipe produces the eigenvalues by itself.

Generally given a real continuous function $f(\phi)$ one forms the Toeplitz elements t_j from it through the Fourier series representation

$$g(\phi) = \sum_{\mu=-\infty}^{\infty} t_\mu \exp(i\,\mu\phi),$$
$$t_\mu = \frac{1}{2\pi}\int_0^{2\pi} g(\phi)\exp(-i\,\mu\phi)\,d\phi\,. \tag{A1}$$

Now a circulant matrix is chosen (see Appendix B) with top row $(c_1, c_2, .., c_n)$ and

$$c_\mu = \frac{1}{n}\sum_{\nu=0}^{n-1} g(2\pi\nu/n)\exp(i2\pi\mu\nu/n). \tag{A2}$$

The circulant matrix's eigenvalues are given exactly by the DFT of this top row,

$$\begin{aligned}\lambda_\nu &= \sum_{\mu=0}^{n-1} c_\mu \exp(-i2\pi\mu\nu/n)\\ &= \frac{1}{n}\sum_{\mu=0}^{n-1}\sum_{\nu=0}^{n-1} g(2\pi\nu/n)\exp\big(i2\pi\mu'\nu/n\big)\exp(-i2\pi\mu\nu/n)\\ &= \sum_{\nu=0}^{n-1} g(2\pi\nu/n)\,\frac{1}{n}\sum_{\mu=0}^{n-1}\exp\big(i2\pi(\mu'-\mu)\nu/n\big)\\ &= g(2\pi\nu/n),\end{aligned} \tag{A3}$$

and they correspond to the discretised function g which was originally Fourier transformed to get the elements c_μ. Now by the Grenander-Szegö theorem for large n the eigenvalues of $\mathbf{C}$ and $\mathbf{T}$ converge, i.e.,

$$\begin{aligned}\lim_{n\to\infty} c_\mu &= \lim_{n\to\infty}\frac{1}{n}\sum_{\nu=0}^{n-1} g(2\pi\nu/n)\exp(i2\pi\mu\nu/n)\\ &= \frac{1}{2\pi}\int_0^{2\pi} g(\phi)\exp(i\,j\phi)\,d\phi\\ &= t_{-\mu}.\end{aligned} \tag{A4}$$

Finally a correspondence needs to be found between the arbitrary function g and the noise directionality. For a function periodic in the interval $-L/2 \le x \le L/2$, Eq. (A1) becomes

$$g'(x) = \sum_{\mu=-\infty}^{\infty} t_\mu \exp(i\,2\pi\mu x/L),$$
$$t_\mu = \frac{1}{L}\int_{-L/2}^{L/2} g'(x)\exp(-i\,2\pi\mu x/L)\,dx\,. \tag{A5}$$

In the current noise case, with directionality $D(s)$ where $s \equiv \sin\theta$ [see Eq. (1)] the equivalent of Eq. (A5) is

$$t_\mu = \int_{-1}^{1} D(s)\exp(ika\mu s)ds. \tag{A6}$$

A comparison of the exponents and integral limits in Eqs. (A5) and (A6) shows that

$$\begin{aligned} &2\pi x/L \equiv ka\, s \equiv ka\, \sin\theta, \\ &2x/L \equiv \frac{f}{f_o}\, s, \\ &L = 2, \\ &s = \sin\theta = xf_o/f, \end{aligned} \tag{A7}$$

where f_o is the design frequency, defined as $f_o = c/(2a)$. Already the equivalences between ν, g, g', and D are as follows:

$$\begin{aligned} &\phi = 2\pi\nu/n, \\ &g(\phi); \quad 0 \le \phi \le 2\pi, \\ &g'(x); \quad -L/2 \le x \le L/2, \\ &D(s); \quad -1 \le s \le 1. \end{aligned} \tag{A8}$$

So one finds that

$$D(s) = D\left(\frac{f_o}{f}x\right) = D\left(\frac{f_o}{f}\frac{\nu}{N}\right). \tag{A9}$$

Thus the spectrum of the eigenvalues of the circulant equivalent of **T** is exactly the n-point discretised noise directionality $D[(f_o/f)(\nu/N)]$ which appears in Eq. (A3) as $g(2\pi\nu/n)$. This can be written as $D(\nu/\nu_o)$ where $\nu_o = Nf/f_o$.

The number of significant values in the eigenvalue spectrum is, by definition, the rank, so finally one arrives at

$$\mathrm{rank}(\mathbf{T}) = 1 + \nu_o \sin\theta_b = 1 + N\frac{f}{f_o}\sin\theta_b, \tag{A10}$$

where the additional one converts $\nu_o \sin\theta_b$ into an index [since $0 \le \nu \le (\mathrm{N}-1)$].

APPENDIX B: SOME CANDIDATE CIRCULANT MATRICES AND THEIR EIGENVALUES

In the noise coherence case the $N \times N$ Toeplitz matrix **T** is Hermitian and positive semi-definite (since the product $\mathbf{v}^\dagger\mathbf{T}\mathbf{v}$ represents a physical power for any steering vector **v**), and we are searching for a set of non-negative (i.e., positive or zero) eigenvalues. Remembering that the Fourier transform of a conjugate-symmetric function is real, a fairly obvious choice of circulant matrix is constructed as follows. Take the first row of **T** (t_1, t_2,..., t_n) and concatenate it with the reversed conjugate offset by one (0, t_n*, t_{n-1}*,..., t_3*, t_2*). With this first row, offsetting subsequent rows each circularly by one element to the right produces a $2N \times 2N$ matrix **C** which is the 2-by-2 block matrix **C** = [**A B; B A**] where **A** ≡ **T** (the given matrix) and the top row of **B** is (0, t_n*, t_{n-1}*,..., t_3*, t_2*). By inspection **C** is circulant, and its first line is conjugate symmetric with a real Fourier transform, therefore its eigenvalues are real, as required.

From the above definition and the properties of circulant matrices the eigenvalues of **C** are given in terms of the elements of **A** by

$$\begin{aligned}
\lambda_\nu^C &= \sum_{\mu=0}^{M-1} C_{0,\mu}\exp(i\,2\pi\,\nu\mu/M) = \sum_{\mu=0}^{N-1} A_{0,\mu}\exp(i\,2\pi\,\nu\mu/M) + \sum_{\mu=N}^{2N-1} B_{0,\mu-N}\exp(i\,2\pi\,\nu\mu/M) \\
&= \sum_{\mu=0}^{N-1} A_{0,\mu}\exp(i\,2\pi\,\nu\mu/M) + 0 + \sum_{\mu=N+1}^{2N-1} A^*_{0,2N-\mu}\exp(i\,2\pi\,\nu\mu/M) \\
&= \sum_{\mu=0}^{N-1} A_{0,\mu}\exp(i\,2\pi\,\nu\mu/M) + \sum_{\mu'=N-1}^{1} A^*_{0,\mu'}\exp(i\,2\pi\,\nu(2N-\mu')/M) \\
&= \sum_{\mu=0}^{N-1} A_{0,\mu}\exp(i\,2\pi\,\nu\mu/M) + \sum_{\mu'=N-1}^{1} A^*_{0,\mu'}\exp(-i\,2\pi\,\nu\mu'/M) \\
&= \sum_{\mu=0}^{N-1} A_{0,\mu}\exp(i\,2\pi\,\nu\mu/M) + \sum_{\mu=1}^{N-1} A^*_{0,\mu}\exp(-i\,2\pi\,\nu\mu/M) \\
&= \sum_{\mu=0}^{N-1} A_{0,\mu}\exp(i\,2\pi\,\nu\mu/M) + \sum_{\mu=0}^{N-1} A^*_{0,\mu}\exp(-i\,2\pi\,\nu\mu/M) - A_{0,0} \\
&= \sum_{\mu=0}^{N-1} \left(A_{0,\mu}\exp(i\,2\pi\,\nu\mu/M) + A^*_{0,\mu}\exp(-i\,2\pi\,\nu\mu/M)\right) - A_{0,0} \\
&= 2\sum_{\mu=0}^{N-1} \left(\mathrm{Re}(A_{0,\mu})\cos(\,2\pi\,\nu\mu/M) + \mathrm{Im}(A_{0,\mu})\sin(\,2\pi\,\nu\mu/M)\right) - A_{0,0} \\
&= 2\,\mathrm{Re}\left(\sum_{\mu=0}^{N-1} A_{0,\mu}\exp(i\,2\pi\,\nu\mu/M)\right) - A_{0,0},
\end{aligned}$$

where $M = 2N$ and $0 \le \nu \le M-1$. This is a standard result for DFTs. The last line is explicitly a length-M DFT but including only N points in the summation. This is the exact equivalent of zero-padding $A_{0,\mu}$ to length $M = 2N$.

By inspection it can be seen that the N-by-N matrix $(\mathbf{A}+\mathbf{B})$ is also circulant, and therefore an alternative candidate for being similar to $\mathbf{T}$. Its eigenvalues are

$$\begin{aligned}
\lambda_\nu^{A+B} &= \sum_{\mu=0}^{N-1}(A_{0,\mu}+B_{0,\mu})\exp(i\,2\pi\,\nu\mu/N) = \sum_{\mu=0}^{N-1}A_{0,\mu}\exp(i\,2\pi\,\nu\mu/N) + \sum_{\mu=0}^{N-1}B_{0,\mu}\exp(i\,2\pi\,\nu\mu/N)\\
&= \sum_{\mu=0}^{N-1}A_{0,\mu}\exp(i\,2\pi\,\nu\mu/N) + \sum_{\mu=1}^{N-1}A^*_{0,N-\mu}\exp(i\,2\pi\,\nu\mu/N)\\
&= \sum_{\mu=0}^{N-1}A_{0,\mu}\exp(i\,2\pi\,\nu\mu/N) + \sum_{\mu=N-1}^{1}A^*_{0,N-\mu}\exp(i\,2\pi\,\nu\mu/N)\\
&= \sum_{\mu=0}^{N-1}A_{0,\mu}\exp(i\,2\pi\,\nu\mu/N) + \sum_{\mu'=1}^{N-1}A^*_{0,\mu'}\exp(i\,2\pi\,\nu(N-\mu')/N)\\
&= \sum_{\mu=0}^{N-1}A_{0,\mu}\exp(i\,2\pi\,\nu\mu/N) + \sum_{\mu'=0}^{N-1}A^*_{0,\mu'}\exp(-i\,2\pi\,\nu\mu'/N) - A_{0,0}\\
&= 2\sum_{\mu=0}^{N-1}(\mathrm{Re}(A_{0,\mu})\cos(\,2\pi\,\nu\mu/N) + \mathrm{Im}(A_{0,\mu})\sin(\,2\pi\,\nu\mu/N)) - A_{0,0}\\
&= 2\,\mathrm{Re}\left(\sum_{\mu=0}^{N-1}A_{0,\mu}\exp(i\,2\pi\,\nu\mu/N)\right) - A_{0,0} = 2\,\mathrm{Re}\left(\sum_{\mu=0}^{N-1}A_{0,\mu}\exp(i\,2\pi(2\,\nu)\mu/M)\right) - A_{0,0}.
\end{aligned}$$

The last line shows explicitly that the eigenvalues of $(\mathbf{A}+\mathbf{B})$ are exactly the even numbered eigenvalues of $\mathbf{C}$.

Although the matrix $(\mathbf{A}-\mathbf{B})$ is not circulant, it can be shown that it is, in fact, skew-circulant (Ng, 2003), and so its eigenvalues can still be written in terms of the DFT of the first row provided that that row is pre-multiplied by $\exp(i\pi\mu/n)$. To be precise, its eigenvalues are

$$\begin{aligned}
\lambda_\nu^{A-B} &= \sum_{\mu=0}^{N-1}(A_{0,\mu}-B_{0,\mu})\exp(i\pi\,\mu/N)\exp(i\,2\pi\,\nu\mu/N) = \sum_{\mu=0}^{N-1}(A_{0,\mu}-B_{0,\mu})\exp(i\pi\,(2\nu+1)\mu/N)\\
&= \sum_{\mu=0}^{N-1}A_{0,\mu}\exp(i\,\pi\,(2\nu+1)\mu/N) - \sum_{\mu=0}^{N-1}B_{0,\mu}\exp(i\,\pi\,(2\nu+1)\mu/N)\\
&= \sum_{\mu=0}^{N-1}A_{0,\mu}\exp(i\,\pi\,(2\nu+1)\mu/N) - \sum_{\mu=1}^{N-1}A^*_{0,N-\mu}\exp(i\,\pi\,(2\nu+1)\mu/N)\\
&= \sum_{\mu=0}^{N-1}A_{0,\mu}\exp(i\,\pi\,(2\nu+1)\mu/N) - \sum_{\mu=N-1}^{1}A^*_{0,N-\mu}\exp(i\,\pi\,(2\nu+1)\mu/N)\\
&= \sum_{\mu=0}^{N-1}A_{0,\mu}\exp(i\,\pi\,(2\nu+1)\mu/N) - \sum_{\mu'=1}^{N-1}A^*_{0,\mu'}\exp(i\,\pi\,(2\nu+1)(N-\mu')/N)\\
&= \sum_{\mu=0}^{N-1}A_{0,\mu}\exp(i\,\pi\,(2\nu+1)\mu/N) - \sum_{\mu'=0}^{N-1}A^*_{0,\mu'}(-1)^{(2\nu+1)}\exp(-i\,\pi\,(2\nu+1)\mu'/N) - A_{0,0}\\
&= \sum_{\mu=0}^{N-1}A_{0,\mu}\exp(i\,\pi\,(2\nu+1)\mu/N) + \sum_{\mu'=0}^{N-1}A^*_{0,\mu'}\exp(-i\,\pi\,(2\nu+1)\mu'/N) - A_{0,0}\\
&= 2\sum_{\mu=0}^{N-1}(\mathrm{Re}(A_{0,\mu})\cos(\,\pi\,(2\nu+1)\mu/N) + \mathrm{Im}(A_{0,\mu})\sin(\,\pi\,(2\nu+1)\mu/N)) - A_{0,0}\\
&= 2\,\mathrm{Re}\left(\sum_{\mu=0}^{N-1}A_{0,\mu}\exp(i\,\pi\,(2\nu+1)\mu/N)\right) - A_{0,0} = 2\,\mathrm{Re}\left(\sum_{\mu=0}^{N-1}A_{0,\mu}\exp(i\,2\pi\,(2\nu+1)\mu/M)\right) - A_{0,0}.
\end{aligned}$$

The last line shows explicitly that the eigenvalues of $(\mathbf{A}-\mathbf{B})$ are exactly the odd numbered eigenvalues of $\mathbf{C}$, so the complete set of eigenvalues of $\mathbf{C}$ consists of the interleaved eigenvalues of $(\mathbf{A}+\mathbf{B})$ and $(\mathbf{A}-\mathbf{B})$.

In contrast, neither **A** nor **B** is circulant. The diagonal of **B** consists entirely of zeros, and so its trace is zero and the sum of its eigenvalues is also zero. Also since trace(**B**) = 0, the sum of the eigenvalues of (**A** + **B**) is identical to the sum of the eigenvalues of **A** since

$$\text{trace}(\mathbf{A}+\mathbf{B}) = \text{trace}(\mathbf{A}) + \text{trace}(\mathbf{B}) = \text{trace}(\mathbf{A}).$$

APPENDIX C: SOME MATRIX INEQUALITY RELATIONS

There are various general inequality relations that help to evaluate the effect on eigenvalues and rank of adding the matrix **H** to the matrix **T** (see Gray, 2006; Ikramov and Nesterenko, 2009). All relate differences of the eigenvalues of (**T** + **H**), λ_i^{T+H}, and **T**, λ_i^T, to the Frobenius norm of **H** [i.e., the matrix difference between (**T** + **H**) and **T**], which is defined here for a matrix **A** with elements $a_{k,j}$ as

$$\|\mathbf{A}\| = \left(\sum_{k=1}^{N}\sum_{j=1}^{N}|a_{k,j}|^2\right)^{1/2}. \tag{C1}$$

Note that, in contrast, Gray's definition has the quantity on the right divided by $N^{1/2}$.

Gray's Lemma 2.4:

$$\frac{1}{\sqrt{N}}\left|\sum_{i=1}^{N}\lambda_i^{T+H} - \sum_{i=1}^{N}\lambda_i^{T}\right| \le \|\mathbf{H}\|.$$

Gray's Lemma 2.5:

$$\frac{1}{\sqrt{N}}\sum_{i=1}^{N}|\lambda_i^{T+H} - \lambda_i^{T}| \le \|\mathbf{H}\|.$$

The Wielandt-Hoffman theorem (Hoffman and Wielandt, 1953):

$$\left(\sum_{i=1}^{N}|\lambda_i^{T+H} - \lambda_i^{T}|^2\right)^{1/2} \le \|\mathbf{H}\|. \tag{C2}$$

The latter theorem is most useful because it enables one to compare the standard deviation of the differences in eigenvalues with the mean of the eigenvalues, as follows. Define the standard deviation σ as

$$\sigma = \left(\frac{1}{N}\sum_{i=1}^{N}|\lambda_i^{T+H} - \lambda_i^{T}|^2\right)^{1/2} \le \left(\frac{1}{N}\sum_{j=1}^{N}\sum_{k=1}^{N}|H_{j,k}|^2\right)^{1/2}$$
$$= \sqrt{N\langle H_{j,k}{}^2\rangle} = \sqrt{N}H_{\text{peak}}/2, \tag{C3}$$

and define the mean μ as

$$\mu = \frac{1}{N}\sum_{i=1}^{N}\lambda_i^T = \frac{\text{trace}(\mathbf{T})}{N} = T_{n,n}. \tag{C4}$$

So their ratio is

$$\frac{\sigma}{\mu} \le \frac{\sqrt{N}}{2}\frac{H_{\text{peak}}}{T_{n,n}}, \tag{C5}$$

and $H_{\text{peak}}/T_{n,n}$ is exactly as calculated in Eq. (13), so

$$\frac{\sigma}{\mu} \le \frac{\sqrt{N}}{4\,kh}. \tag{C6}$$

At 3 kHz with 32 hydrophones set 20 m above the seabed the limit on σ/μ is 1/178.

A more stringent restriction on the deviation of individual eigenvalues is set by the Weyl inequality (Franklin, 1993). In the current notation it is

$$\lambda_i^T + \lambda_N^H \le \lambda_i^{T+H} \le \lambda_i^T + \lambda_1^H. \tag{C7}$$

Knowing that the eigenvalues of **H** are bounded by $\|\mathbf{H}\|$ which can be written [from Eq. (C3)] as $NH_{\text{peak}}/2$, this becomes

$$|\lambda_i^{T+H} - \lambda_i^T| \le NH_{\text{peak}}/2. \tag{C8}$$

Using Eq. (C4) this can be rearranged in terms of the mean eigenvalue, μ, as

$$\frac{|\lambda_i^{T+H} - \lambda_i^T|}{\mu} \le \frac{N}{2}\frac{H_{\text{peak}}}{T_{n,n}}, \tag{C9}$$

or alternatively in terms of the first (maximum) eigenvalue as

$$\frac{|\lambda_i^{T+H} - \lambda_i^T|}{\lambda^T{}_1} \le \frac{\nu_o}{2}\frac{H_{\text{peak}}}{T_{n,n}} = \frac{Nf}{2f_o}\frac{H_{\text{peak}}}{T_{n,n}} = \frac{Nf}{4khf_o}, \tag{C10}$$

where ν_o is the effective number of eigenvalues as defined in Eq. (3) of the main text. At 3 kHz with a 32 hydrophone array (design frequency $f_o = 4167$ Hz) set 20 m above the seabed the limit on the fractional deviation of individual eigenvalues is 1/43. This constrains the magnitude of λ_n^{T+H} but it also prevents any significant increase in the number of eigenvalues over and above those of **T** alone. Thus **H** has minimal effect on the rank of **T** + **H**.

Ainslie, M. A. (**2010**). *Principles of Sonar Performance Modelling* (Springer-Verlag, Berlin), pp. 414–431.

Buckingham, M. J. (**1980**). "A theoretical model of ambient noise in a low-loss shallow water channel," J. Acoust. Soc. Am. **67**, 1186–1192.

Cron, B. F., and Sherman, C. H. (**1962**). "Spatial correlation functions for various noise models," J. Acoust. Soc. Am. **34**, 1732–1736.

Fang, G., Qiu, S., Ma, X., Sheng, W., and Han, Y. (**2014**). "Robust adaptive beamforming based on fast rank-reducing MVB algorithm," in *IEEE Antennas and Propagation (APCAP), 3rd Asia-Pacific Conference*, pp. 317–320.

Franklin, J. N. (**1993**). *Matrix Theory* (Dover Publications, Mineola, NY), pp. 157–161.

Gentle, J. E. (**1998**). "Cholesky factorization," in *Numerical Linear Algebra for Applications in Statistics* (Springer-Verlag, New York), Sec. 3.2.2, pp. 93–95.

Goldstein, J. S., and Reed, I. S. (**1997**). "Reduced-rank adaptive filtering," IEEE Trans. Signal Process. **45**, 492–496.

Gray, R. M. (**1972**). "On the asymptotic eigenvalue distribution of Toeplitz matrices," IEEE Trans. Inf. Theory **IT-18**, 725–730.

Gray, R. M. (**2006**). "Toeplitz and circulant matrices: A review," Found. Trends Commun. Inf. Theory **2**(3), 155–239.

Grenander, U., and Szegö, G. (**1958**). *Toeplitz Forms and their Applications* (University of California Press, Berkeley and Los Angeles), pp. 1–245.

Harrison, C. H. (**1996**). "Formulas for ambient noise level and coherence," J. Acoust. Soc. Am. **99**, 2055–2066.

Harrison, C. H. (**2004**). "Drifting MF vertical array measurements in the 'noise-notch,' " NATO Undersea Research Centre, Viale San Bartolomeo 400, 19126 La Spezia, Italy. NURC Report SM-434, December 2004 (unclassified).

Harrison, C. H. (**2005**). "Performance and limitations of spectral factorization for ambient noise sub-bottom profiling," J. Acoust. Soc. Am. **118**, 2913–2923.

Harrison, C. H. (**2008**). "Target detection and location with ambient noise," J. Acoust. Soc. Am. **123**, 1834–1837.

Harrison, C. H. (**2010**). "An approximate form of the Rayleigh reflection loss and its phase: Application to reverberation calculation," J. Acoust. Soc. Am. **128**, 50–57.

Harrison, C. H. (**2017**). "Separation of measured noise coherence matrix into Toeplitz and Hankel parts," J. Acoust. Soc. Am. **141**, 2812–2820.

Harrison, C. H., and Siderius, M. (**2008**). "Bottom profiling by correlating beam-steered noise sequences," J. Acoust. Soc. Am. **123**, 1282–1296.

Harrison, C. H., and Simons, D. G. (**2002**). "Geoacoustic inversion of ambient noise: A simple method," J. Acoust. Soc. Am. **112**, 1377–1389.

Hoffman, A. J., and Wielandt, H. W. (**1953**). "The variation of the spectrum of a normal matrix," Duke Math. J. **20**, 37–39.

Ikramov, Kh. D., and Nesterenko, Yu. R. (**2009**). *Theorems of the Hoffman–Wielandt Type for the Coneigenvalues of Complex Matrices* (Pleiades Publishing, Moscow), Vol. 80, pp. 536–540.

Kuperman, W. A., and Ingenito, F. (**1980**). "Spatial correlation of surface-generated noise in a stratified ocean," J. Acoust. Soc. Am. **67**, 1988–1996.

Ng, M. K. (**2003**). "Circulant and skew-circulant splitting methods for Toeplitz systems," J. Comp. Appl. Math. **159**, 101–108.

Quijano, J. E., Dosso, S. E., Dettmer, J., Zurk, L. M., and Siderius, M. (**2012**). "Trans-dimensional geoacoustic inversion of wind-driven ambient noise," J. Acoust. Soc. Am. **133**, EL47–EL53.

Ricks, D. C., Cifuentes, P. G., and Goldsein, J. S. (**2001**). "Adaptive beamforming using the multistage Wiener filter with a soft stop," in *IEEE Signals, Systems and Computers, Conference Record of the Thirty-Fifth Asilomar Conference* (November 4–7), Vol. 2, pp. 1401–1406.

Siderius, M., Harrison, C. H., and Porter, M. B. (**2006**). "A passive fathometer technique for imaging seabed layering using ambient noise," J. Acoust. Soc. Am. **120**, 1315–1323.

Siderius, M., Song, H., Gerstoft, P., Hodgkiss, W. S., Hursky, P., and Harrison, C. (**2010**). "Adaptive passive fathometer processing," J. Acoust. Soc. Am. **127**, 2193–2200.

Traer, J., and Gerstoft, P. (**2011**). "Coherent averaging of the passive fathometer response using short correlation time," J. Acoust. Soc. Am. **130**, 3633–3641.

Yardim, C., Gerstoft, P., Hodgkiss, W., and Traer, J. (**2014**). "Compressive geoacoustic inversion using ambient noise," J. Acoust. Soc. Am. **135**, 1245–1255.

Document Data Sheet

Security Classification		Project No.
Document Serial No.	**Date of Issue**	**Total Pages**
CMRE-PR-2019-031	May 2019	15 pp.

Author(s)

Chris H. Harrison

Title

The ocean noise coherence matrix and its rank

Abstract

An expression for the cross-spectral density matrix of ocean noise naturally separates into a Toeplitz part and a Hankel part [Harrison (2017). J. Acoust. Soc. Am. 141, 2812–2820]. The Toeplitz part is shown to be substantially rank-deficient for all practical acoustic cases, which has implications for adaptive beam forming. The influence of the Hankel part on passive fathometry is investigated, and its effect on adaptive beam forming is shown to be weak or negligible. Numerical demonstrations of these findings including beam patterns and eigenvalue spectra derived via circulant matrices are given based on a simple half-space with a Rayleigh reflection coefficient. Two sets of experimental data are revisited in this context, deriving eigenvalue spectra, beam patterns, and passive fathometry impulse responses with conventional and adaptive processing and differing amounts of averaging. The solution to a long-standing puzzle of processing inconsistency is suggested.

Keywords

Issuing Organization

NATO Science and Technology Organization
Centre for Maritime Research and Experimentation

Viale San Bartolomeo 400, 19126 La Spezia, Italy

[From N. America:
STO CMRE
Unit 31318, Box 19, APO AE 09613-1318]

Tel: +39 0187 527 361
Fax:+39 0187 527 700

E-mail: library@cmre.nato.int